Hindawi
Computational Intelligence and Neuroscience
Volume 2022, Article ID 3024590, 14 pages
https://doi.org/10.1155/2022/3024590

Research Article

A Hybrid Matching Network for Fault Diagnosis under Different Working Conditions with Limited Data

Qiuchen He,[1] **Shaobo Li**,[1,2] **Chuanjiang Li**,[1] **Junxing Zhang**,[2] **Ansi Zhang**,[1,2] **and Peng Zhou**[1]

[1]*School of Mechanical Engineering, Guizhou University, Guiyang 550025, China*
[2]*State Key Laboratory of Public Big Data, Guizhou University, Guiyang 550025, China*

Correspondence should be addressed to Shaobo Li; lishaobo@gzu.edu.cn

Received 9 November 2021; Revised 18 April 2022; Accepted 13 June 2022; Published 1 July 2022

Academic Editor: Yugen Yi

Intelligent fault diagnosis methods based on deep learning have achieved much progress in recent years. However, there are two major factors causing serious degradation of the performance of these algorithms in real industrial applications, i.e., limited labeled training data and complex working conditions. To solve these problems, this study proposed a domain generalization-based hybrid matching network utilizing a matching network to diagnose the faults using features encoded by an autoencoder. The main idea was to regularize the feature extractor of the network with an autoencoder in order to reduce the risk of overfitting with limited training samples. In addition, a training strategy using dropout with random changing rates on inputs was implemented to enhance the model's generalization on unseen domains. The proposed method was validated on two different datasets containing artificial and real faults. The results showed that considerable performance was achieved by the proposed method under cross-domain tasks with limited training samples.

1. Introduction

Mechanical fault diagnosis plays a significant role in modern industry. Failures of machines are likely to result in an entire mechanical system collapse and production line downtime, as well as serious economic losses. Timely and accurate fault diagnosis has become an indispensable technology in modern industries to ensure the safe and reliable operation of mechanical systems [1–3].

Recently, deep learning has achieved considerable progress in computer vision [4, 5], speech and natural language processing [6], product defect detection [7], and road planning [8]. Expectedly, an increasing number of researchers have applied deep learning techniques to fault diagnosis and proposed intelligent fault diagnosis methods [9–16]. Hasan et al. [17] proposed an explainable AI-based model for bearings fault diagnosis. Sun et al. [18] developed a sparse autoencoder-based deep neural network for the fault diagnosis of induction motors, which realized accurate fault prediction. Li et al. [19] designed a two-layer Boltzmann machine to develop representations of the statistical parameters of wavelet packet transform for gearbox fault diagnosis. Ding et al. [20] applied a deep convolutional neural network (CNN) by using wavelet packet energy as the input to develop a bearing fault diagnosis system, with which they obtained reasonable fault detection performance. Zhang et al. [21] proposed a method based on deep learning that uses raw temporal signals as input, which achieved high accuracy under noisy conditions. Qiao et al. [22] built a dual-input model and achieved satisfactory antinoise and load adaptability based on a CNN and a long short-term memory neural network. The deep learning methods have discarded the traditional time-consuming and unreliable manual analysis, improving the efficiency of fault diagnosis [23–28] considerably.

Traditional deep learning methods can only achieve satisfactory results when the training set (source domain) and the test set (target domain) are in the same data distribution. In practical applications, however, due to the complexity of the working conditions of the mechanical system (load, motor speed, etc.), the training set and the testing set may have distinct distributions. The predictive performance of the deep learning models is greatly affected by these facts. To face this challenge, some transfer learning algorithms have been proposed to enhance the domain adaptability of the model. Zhang et al. [21] presented a novel algorithm based on deep learning to alleviate the degradation of the performance of intelligent fault diagnosis under noisy environments and different working loads. Yao et al. [29] designed a new model based on a Stacked Inverted Residual Convolution Neural Network to ensure the accuracy of the model in noisy environments. Hu et al. [30] proposed a data augmentation algorithm and presented a self-adaptive neural network to boost models' generalization ability. Lu and Yin [31] developed a transferable common feature space mining algorithm to extract the common features from multidomain data. Wu et al. [32] constructed a few-shot transfer learning method in variable conditions. Wei et al. [33] proposed multiple source domain adaptation methods to extract condition-invariant features for fault diagnosis.

Aside from the obstacle posed by cross-domain tasks, a limited training set is another challenge that restricts the practical application of deep learning fault diagnosis algorithms. Most of the deep learning methods require a large amount of labeled data for model training. However, in actual industrial application scenarios, collecting a huge amount of labeled data for every type of failure under each working condition poses a considerable challenge. To address this problem, some studies on mechanical fault diagnosis using limited labeled training data have been conducted. Wang et al. [34] presented an integrated fault prognosis and diagnosis method for the predictive maintenance of turbine bearings, which achieved reasonable performance under limited labeled data. Zhang et al. [35] applied the few-shot approach for fault diagnosis and designed an artificial neural network based on a Siamese network, achieving interesting results with limited data. Li et al. [36] designed a meta-learning fault diagnosis method (MLFD) framework using model-agnostic meta-learning, which has performed excellently under complex working conditions. Hang et al. [37] applied a two-step clustering algorithm and principal component analysis to improve classification performance in the case of unbalanced high-dimensional data. Li et al. [38] proposed a deep, balanced domain adaptation neural network, which achieved satisfactory results with limited labeled data. Duan et al. [39] proposed a novel data description support vector based on deep learning for unbalanced datasets.

As two important research directions of fault diagnosis, improving the model's generalization to new domains and performance under limited training samples has made good progress, respectively. However, the reports of studies combining these two directions are relatively rare to find. In this study, to achieve domain generalization under limited training samples, we proposed a hybrid matching network (HMN) designed by connecting a prototypical network to the bottleneck of an autoencoder for fault diagnosis to unseen domains with limited training samples.

Our model mainly consists of two parts: (1) the autoencoder regularizing the feature extractor of the model to reduce the risk of overfitting and (2) the matching network achieving the measurement of samples similarity. Besides, a novel strategy is implemented in the training process to improve the model's domain generalization.

The main contributions of this study can be summarized as follows:

(1) A novel fault diagnosis method based on matching network and autoencoder, known as HMN, was proposed to face the cross-domain scenarios. In the tasks, the model was training on the source domain with limited data and testing on the unseen target domains without access to their distributions.

(2) Dropout on the input layer with randomly changing rates was employed to improve the generalization ability of the model. Autoencoder was built to reduce the risks of model overfitting with limited training samples by regularizing the feature extractor of the network.

(3) The well-designed algorithm can effectively cope with domain generalization (DG) fault diagnosis. Comprehensive experiments were designed and executed to prove the effectiveness of the proposed HMN with two bearing faults datasets containing artificial and real faults.

The rest of the paper is organized as follows. Autoencoder and prototypical networks are introduced in Section 2. Section 3 describes the proposed method in detail. Section 4 presents the experiments, results, and discussion. Finally, the conclusions are drawn in Section 5.

2. Autoencoder and Prototypical Network

2.1. Autoencoder. Autoencoder, an unsupervised learning method, uses a neural network to implement the representation learning task. Specifically, a neural network architecture designed to impose a bottleneck layer forces a compressed knowledge representation of the original input.

As shown in Figure 1, the autoencoder is mainly composed of two parts: an encoder and a decoder. The encoder function, which is denoted as f_θ, enables the efficient computation of a feature vector $h = f_\theta(x)$ from an input vector x. It is important to note that the dimensions of h are usually lower than the dimensions of x. Another parameterized function g_θ, known as the decoder, maps the feature vector back to the input space, generating a reconstruction vector $\widehat{x} = g_\theta(h)$.

A simplified autoencoder structure can be represented as a fully connected neural network with three layers, i.e., an input layer, a bottleneck layer, and an output layer. The parameter sets of the encoder and the decoder are trained simultaneously when performing the task of reconstructing the input as much as possible, i.e., minimizing reconstruction error $L(x, \widehat{x})$ which is usually described by MSE over training examples. For a training set $\{x^{(i)}\}_{i=1}^{n}$, the reconstruction error of MSE is expressed as follows:

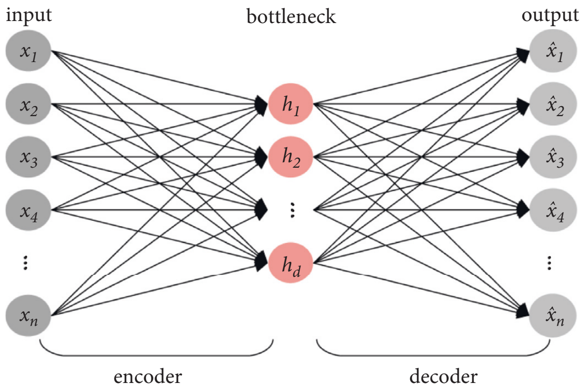

Figure 1: The typical architecture of a simple autoencoder.

$$J_{\mathrm{MES}}(\theta) = \frac{1}{n}\sum_{i=1}^{n}\left(\frac{1}{2}\left|x^{(i)} - \widehat{x}^{(i)}\right|\right). \tag{1}$$

If the input is normalized to $[0,1]$, the cost function can be described as binary cross-entropy, which comes in the form below:

$$J_{\mathrm{bc}}(\theta) = \frac{1}{\mathrm{nm}}\sum_{i=1}^{n}\sum_{j=1}^{m}\left[x_j^{(i)}\log\widehat{x}_j^{(i)} + \left(1 - x_j^{(i)}\right)\log\left(1 - \widehat{x}_j^{(i)}\right)\right], \tag{2}$$

where $x_j^{(i)}$ and $\widehat{x}_j^{(i)}$ represent the j th element of $x^{(i)}$ and $\widehat{x}^{(i)}$, respectively, n and m represent the batch size and the dimension of x, respectively.

Using penalizing parameters based on reconstruction errors, the network can learn about the most important attributes of the input data and how to best reconstruct the input from the feature vector.

2.2. Prototypical Networks. Prototypical Networks [40] have been proposed for few-shot learning, which requires only a small amount of training data with limited information, as compared to traditional machine learning methods requiring a large amount of data to train a model for good results. As shown in Figure 2, the classification task can be achieved by comparing the distances with mean representations of each class in the metric space produced by Prototypical Networks.

Specific to a few-shot task, given a support set that has M labeled samples $S = \{(x_1, y_1), \ldots, (x_M, y_M)\}$, $x_i \in R^D$ is a vector with D-dimension and $y_i \in \{1, \ldots, K\}$ is the label of each class, S_k describes the set labeled with k. A representation c_k, or prototype, of each class is computed by meaning the support points belonging to class k:

$$c_k = \frac{1}{|S_k|}\sum_{(x_i, y_i)\in S_k} f_\theta(x_i), \tag{3}$$

where f_θ is an embedding function with learnable parameters θ. For a function computing distance $d = R^D \times R^D \longrightarrow [0, +\infty)$, distribution of a query point x_q over distances to all prototypes of each class in the metric space is computed by prototypical networks:

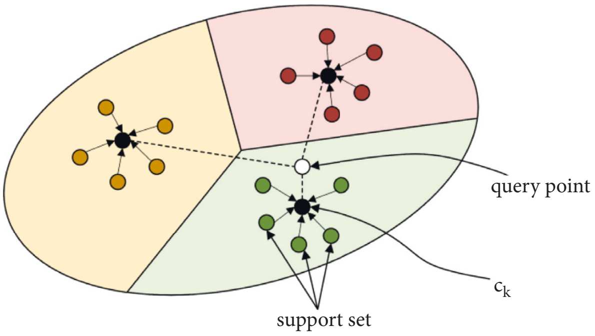

Figure 2: Prototypical network. Prototypes c_k are the mean of the embedded support points. The embedded query points are classified via a softmax over distances to each prototype.

$$p_\theta(y = k \mid x_q) = \frac{\exp\left(-d\left(f_\theta(x_q), c_k\right)\right)}{\sum_{k'}\exp\left(-d\left(f_\theta(x_q), c_{k'}\right)\right)}. \tag{4}$$

Train the network by minimizing $L(\theta) = -\log p_\theta(y = k \mid x_q)$, the loss of the k class.

3. Methods

The proposed HMN for fault diagnosis is described in detail in this section. As shown in Figure 3, our model has both one-input and two-output configurations. One of the outputs was the reconstruction of the input, and the other was the prediction of health conditions using a prototypical network. The details of the model are illustrated in Table 1.

3.1. Data Preprocessing. The proposed model used the short-time spectrogram as a 2D input. Firstly, as shown in Figure 4, the sliding window of 2048 points generated the samples. Secondly, STFT used a fixed-length nonzero window function to slide along the time axis, truncating the source signal into segments of equal length. Assuming that these segments are stable, Fourier transform can be used to obtain the local frequency spectra of the segments. And finally, these local frequency spectra were recombined along the time axis to obtain a 2D time-frequency graph. The formula is presented in equation (5) as below:

$$\mathrm{STFT} = \int_{-\infty}^{+\infty} x(t)g(t - \tau)e^{-j\omega t}d\tau, \tag{5}$$

where $x(t)$ is the original timing signal and $g(t - \tau)$ is the window function applied as the center point at time τ. In this study, the Hann window was used. To speed up the convergence of the model, we converted 2D spectrogram into a grayscale image with a value between 0 and 1. This process can be expressed as follows:

$$X'(\tau, \omega) = \frac{|X(\tau, \omega)| - |X(\tau, \omega)|_{\min}}{|X(\tau, \omega)|_{\max} - |X(\tau, \omega)|_{\min}}, \tag{6}$$

where $|X(\tau, \omega)|$ is the element magnitude, $|X(\tau, \omega)|_{\min}$ and $|X(\tau, \omega)|_{\max}$ represent the minimum and maximum magnitude, respectively. Finally, the normalized spectrogram

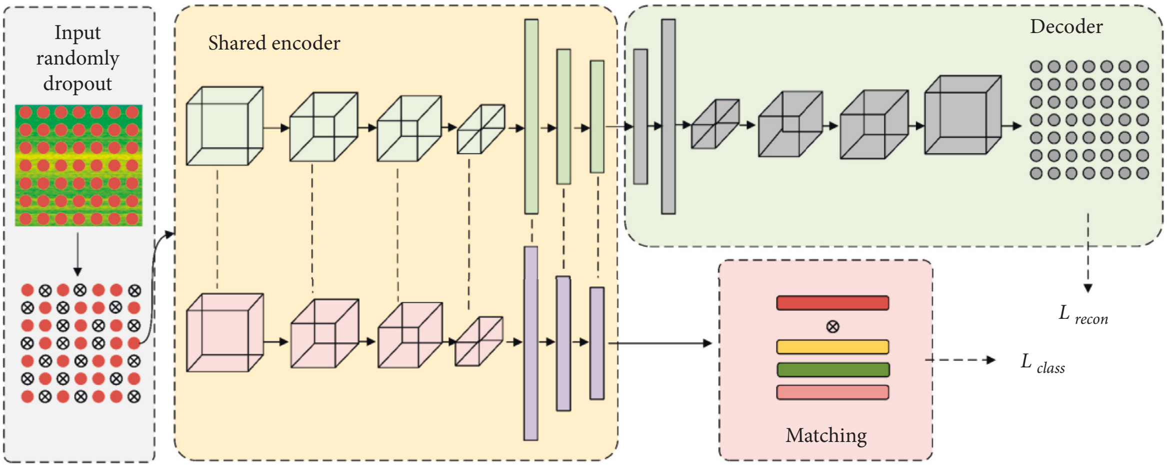

Figure 3: The architecture of the proposed model.

Table 1: The details of the proposed networks.

Module	Layer	Layer type	Filter size/stride/channels (neurons)	Kernel number	Output size (Width * Depth)
Shared encoder	1	Input	—	—	64 * 64 * 1
	2	Convolution	3 * 3/2	16	32 * 32 * 16
	3	Convolution	3 * 3/2	32	16 * 16 * 32
	4	Convolution	3 * 3/2	32	8 * 8 * 32
	5	Convolution	3 * 3/2	32	4 * 4 * 32
	6	Flatten	—	—	512
	7	Fully connected	64	—	64
	8	Fully connected	32	—	32
Decoder	9	Fully connected	64	—	64
	10	Fully connected	512	—	512
	11	Reshape	—	—	4 * 4 * 32
	12	Transposed convolution	3 * 3/2	32	8 * 8 * 32
	13	Transposed convolution	3 * 3/2	32	16 * 16 * 32
	14	Transposed convolution	3 * 3/2	32	32 * 32 * 16
	15	Transposed convolution	3 * 3/2	1	64 * 64 * 1
Matching	16	Prototypical loss	—	—	—

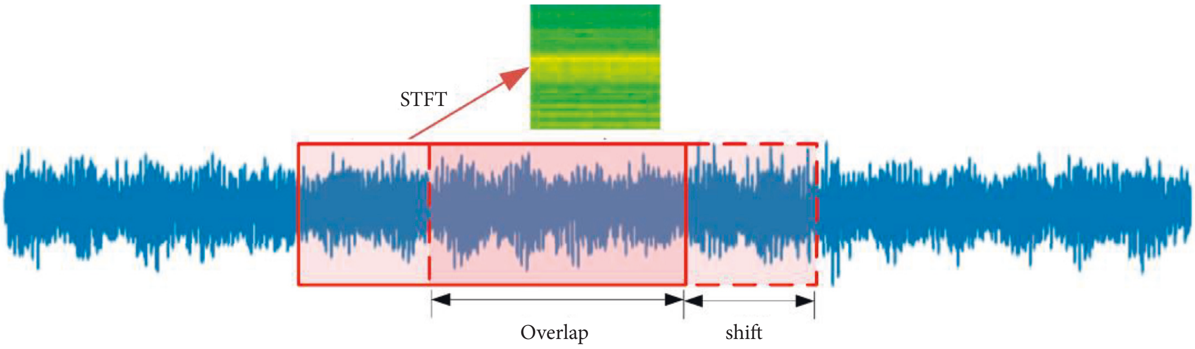

Figure 4: The vibration signal is sliced into samples containing 2048 points.

$X'(\tau, \omega)$ was compressed into 64×64 time-frequency graphs as the input of the model.

3.2. Random Dropout on Input. Dropout is a technique proposed in [41] to prevent the deep neural nets from overfitting. The key idea is to randomly deactivate the units along with their connections from the network with probability p during training, preventing units from coadapting too much. Applying dropout amounts to sampling a "thinned" network from the original one during training. During the testing phase, dropout is disabled, which can be seen as an average of the predictions of many "thinned" networks. The networks trained with dropout usually have much better generalization ability on supervised learning tasks.

The deactivated units affect all the ones in the network, including the layers with dropout. Dropout applied in the lower layers can also be seen as providing noisy inputs for the higher layers. It can be interpreted as a method of data augmentation by adding noise to its hidden layers.

Adding noise with a specific distribution was not enough. Inspired by [21], we randomly changed the dropout rate during the training to obtain noise with the uncertain feature. Specifically, in each batch of training, the dropout rate was a random value between 0.1 and 0.9. The visualization of the operation is illustrated in Figure 5.

$$\begin{aligned} p &\sim \text{Uniform}(0.1, 0.9), \\ r_i &\sim \text{Bernoulli}(p), \\ \widehat{x} &= r_i * x. \end{aligned} \tag{7}$$

Here $*$ denotes an elementwise product. r_i is a vector whose elements follow independent Bernoulli random variable which has a probability p. x and $\widehat{x}$ are the raw input and the interfered output of x.

The purpose of adding dropout to the input layer was to add masking noise to the input, making the model insensitive to disturbance and improving the domain generalization of the model.

3.3. Feature Extraction. To make full use of unlabelled information, an autoencoder was designed for feature extraction. In the encoding stage, the 2D time-frequency images first passed through a set of 2D convolutional layers. The 2D convolutional layers captured the localized features of the image well due to its translation invariance. To obtain more diverse features at the same feature level, the weights in the convolutional layer were designed as a series of 2D filters. Each filter convolves independently across the input feature map in the forward pass, obtaining the output of one of the convolution layer's channels. Generally, the computing of the convolutional layer l is expressed as follows:

$$Z_c^l = f^l\left(\sum_{i=1}^{c^{l-1}} W_{i,c}^l * Z_i^{l-1} + b_c^l\right), \tag{8}$$

where $*$ operator denotes the convolution of the channel i of the feature matrix Z_i^{l-1} and the kernel $W_{i,c}^l$, which produces the feature map Z_c^l of the c^{th} channel of the layer l. b_c^l is the bias of c^{th} channel in the layer l. The $f^l(\cdot)$, a nonlinear activation function using RELU in this study is implemented on the final output of the convolution network.

The encoder and decoder were designed in a symmetrical form. To reconstruct the coding of the bottleneck layer to the same size as the input time-frequency image, a transposed convolution layer was used in the decoder to unsampled the feature map. Following [42], the encoder contained four convolution layers and two fully connected layers, while the decoder contained four transposed convolution layers and two fully connected layers.

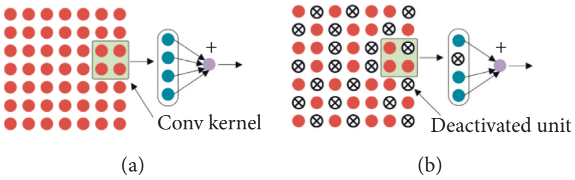

Figure 5: Input dropout:(a) without dropout, (b) with dropout.

3.4. Training of the Proposed Model. The two outputs of the model correspond to two different losses, including the reconstruction loss L_r computed by the autoencoder and the classification loss L_c computed by the prototype network. In the training process, L_r and L_c are minimized. The total loss in the model training can be described as follows:

$$L = L_c + \alpha L_r, \tag{9}$$

where the hyperparameter α is the weight coefficient used to adjust the weights of different losses. In the training process, the network is optimized with an Adam optimizer which sets the learning rates for each parameter adaptively. The steps of the proposed training algorithm are listed in Algorithm 1.

4. Experiments, Results, and Discussion

4.1. Experiment Setup

4.1.1. Experiment Description. To verify the validity of our method, experiments are carried out on two bearing datasets selected from the Case Western Reserve University (CWRU) bearing datasets [43] and Paderborn bearing dataset [44]. We assume the source domain contains limited labeled samples and set 6, 10, 15, 50, 100, 200, 300, 500, 600 training samples per class to test the performance of the proposed method. Fivefold cross-validation is applied to the experiments. The test platform uses an Ubuntu 18.04 + Python 3.6 + Pytorch with an Intel® CORE™ i7-9750H CPU and a Nvidia GTX 1080Ti GPU.

4.1.2. Comparison Methods and Evaluation Metrics. To verify the advantages of the proposed model, as shown in Table 2, several popular models are compared, using three types of time series input methods (Siamese-based CNN [35], PSDAN [45], and WDCNN [46]) and three types of time-frequency input methods (SCNN, HCAE [42],s and DeIN [47]). The Siamese-based CNN was designed by [35]. PSADAN was an adversarial domain adaptation method. WDCNN, in which a wide convolution kernel was used in the front of the network, was proposed in [46]. DeIN was proposed in [47]. SCNN is a common CNN that follows a softmax at the end of the same structure with the encoder of HMN. The HCAE was proposed in [42]. The HMN model was proposed by our team.

All the models are trained in the source domain and tested in the unseen target domain. For the sake of fair comparison, the hyperparameters of models are carefully selected.

```
Initialize: weight coefficient $\alpha = 0.5$, the batch size is set to 8, the learning rate $\eta$ is set to 0.0001, and the epoch is set to 300
for $n = 0, \ldots,$ epoch do
  for $i = 0, \ldots,$steps do
    input a batch samples from the source domain
    random sampling $p$ from Uniform (0.1, 0.9)
    dropout on inputs with rate $p$
    compute prototypes $c_k$
    $L = L_c + \alpha L_r$,
    $\theta \longleftarrow \theta - \eta (\partial L_c / \partial\theta + \alpha \partial L_r / \partial\theta)$
  end for
end for
```

Algorithm 1: The proposed training algorithm.

Table 2: Details of the comparison methods.

Input type	Method name	Implementation details
Time-based	Siamese based CNN	Details referred to [35]
	PSDAN	Implementation details referred to [45]
	WDCNN	Details referred to [46]
Time-frequency	SCNN	The encoder of HMN connecting softmax regression.
	HCAE	Implementation details referred to [42]
	DeIN	Details referred to [47]
	HMN (our)	As shown in Table 1

Table 3: Description of CWRU bearing datasets.

Fault location		None	Ball			Inner race			Outer race			Load
Fault Diameter(inch)		0	0.007	0.014	0.021	0.007	0.014	0.021	0.007	0.014	0.021	
Class labels		1	2	3	4	5	6	7	8	9	10	
Dataset A	Train	600	600	600	600	600	600	600	600	600	600	1
	Test	25	25	25	25	25	25	25	25	25	25	
Dataset B	Train	600	600	600	600	600	600	600	600	600	600	2
	Test	25	25	25	25	25	25	25	25	25	25	
Dataset C	Train	600	600	600	600	600	600	600	600	600	60 0	3
	Test	25	25	25	25	25	25	25	25	25	25	

Several evaluation indicators are used to evaluate the performance of the proposed model in the following aspects: (1) accuracy, (2) precision, (3) $F1$ score ($F1$), and average $F1$ score ($\alpha F1$). Precision, $F1$, and αF can be obtained using the following equations:

$$\text{Precision} = \frac{\text{TP}}{\text{TP} + \text{FP}},$$
$$F1 = \frac{2\text{TP}}{2\text{TP} + \text{FN} + \text{FP}}, \qquad (10)$$
$$\alpha F1 = \frac{\sum F1}{\text{Total\_classes}},$$

where TP, FP, and FN represent true positive, false positive, and false negative, respectively.

4.2. Case Study 1: CWRU Bearing Datasets

4.2.1. Data Description. In the CWRU bearing datasets [43], the 12k drive end fault data were selected as the original experimental data. Four types of faults, i.e., normal, ball fault, inner race fault, and outer race fault, were found in these data, as shown in Table 3. Each fault type had three different subtypes, i.e., 0.007 inches, 0.014 inches, and 0.021 inches. Thus, there were altogether 10 different types of fault.

Signals of all fault types are shown in Figure 6. Each type of fault had three different loads, i.e., 1, 2, and 3 hp (motor speed of 1772, 1750, and 1730 RPM), as illustrated in Table 4. During data collection, each sample was collected from a vibration signal, as shown in Figure 7. Half of the signals were used to generate training data, and the remaining signals were used to generate the test set. As shown in

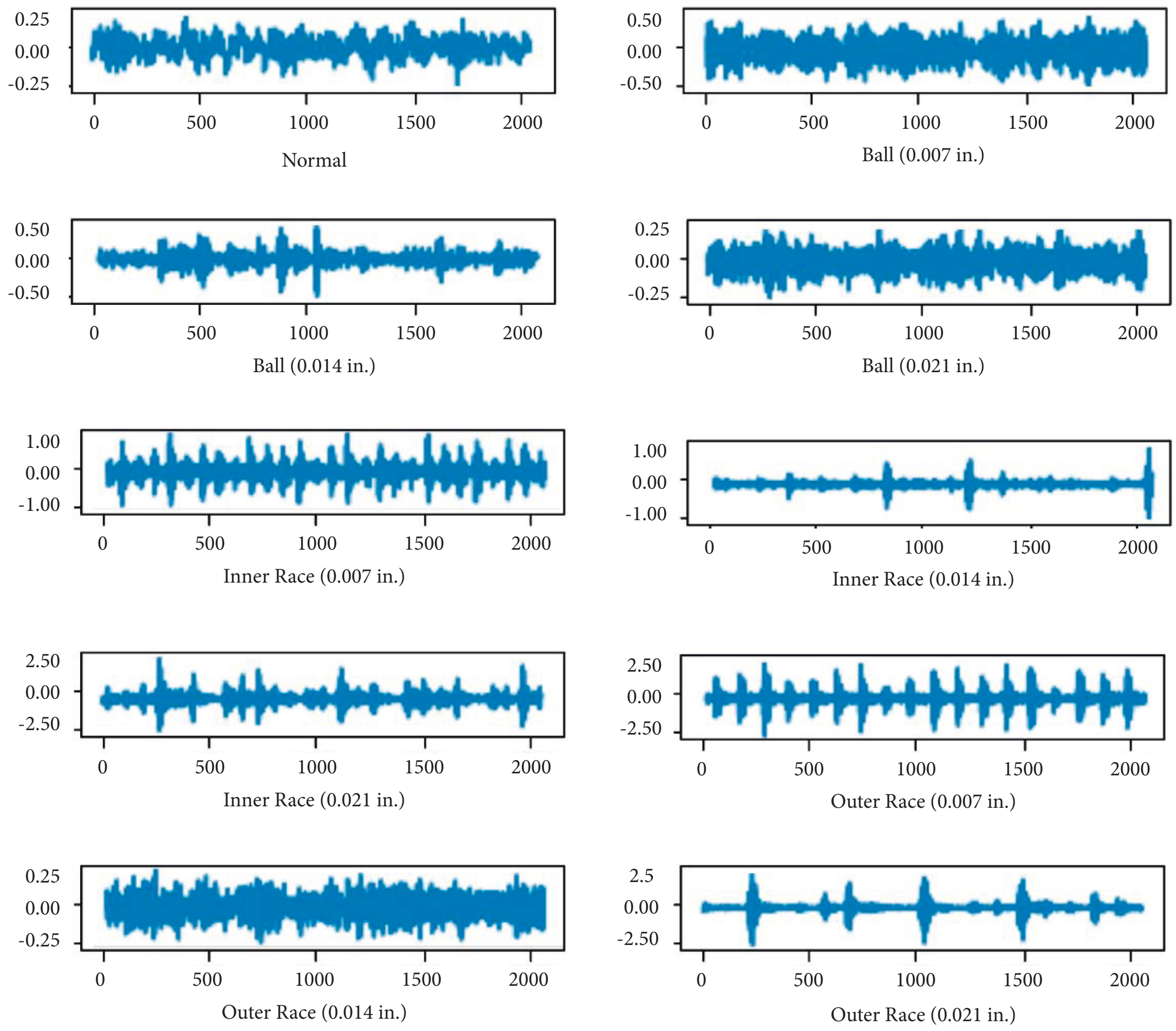

Normal

Ball (0.007 in.)

Ball (0.014 in.)

Ball (0.021 in.)

Inner Race (0.007 in.)

Inner Race (0.014 in.)

Inner Race (0.021 in.)

Outer Race (0.007 in.)

Outer Race (0.014 in.)

Outer Race (0.021 in.)

Figure 6: Vibration signals corresponding to 10 states.

Table 4: Three different working conditions.

Datasets	Load/HP	Rotational speed/rpm	Damage size/10^{-3}in
A	1	1772	7, 14, 21
B	2	1750	7, 14, 21
C	3	1730	7, 14, 21

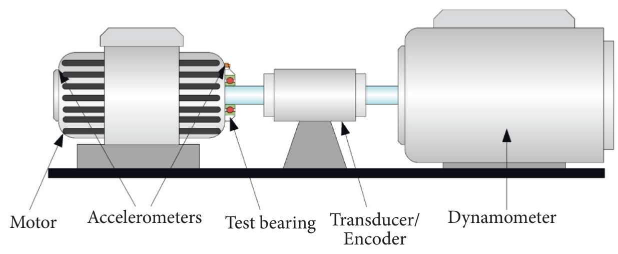

Figure 7: CWRU. Bearing fault diagnosis test rig.

Figure 4, the training samples were generated using 2048 points sliding window with 80 points overlapping steps. The test set samples passed through sliding windows in the same size, but the samples were generated without overlapping.

We set the data under different working conditions as experimental data. Datasets A, B, and C correspond to different working conditions with loads of 1, 2, and 3 hp, respectively. Each dataset contained 6000 training samples and 250 test samples.

4.2.2. Results and Analysis. Figure 8 illustrates the accuracy of all methods of training with various amounts of samples. With outstanding performance, HMN is evidently superior to the other approaches. We can find that cross-domain task C to A is the most difficult, in which even with sufficient training samples, the accuracy of four compared methods does not reach 90%, but the proposed model still achieves satisfactory results.

The results of training with 6 samples per class were observed. The classification accuracies of the cross-domain tasks are shown in Table 5. The best performance was achieved using HMN among all the methods in all the scenarios. Specifically, HMN achieved an accuracy of 92.65% in C-A, which was 34.61%, 21.57%, 26.38%, 19.32%, 40.21%, and 27.09% higher than DeIN, Siamese

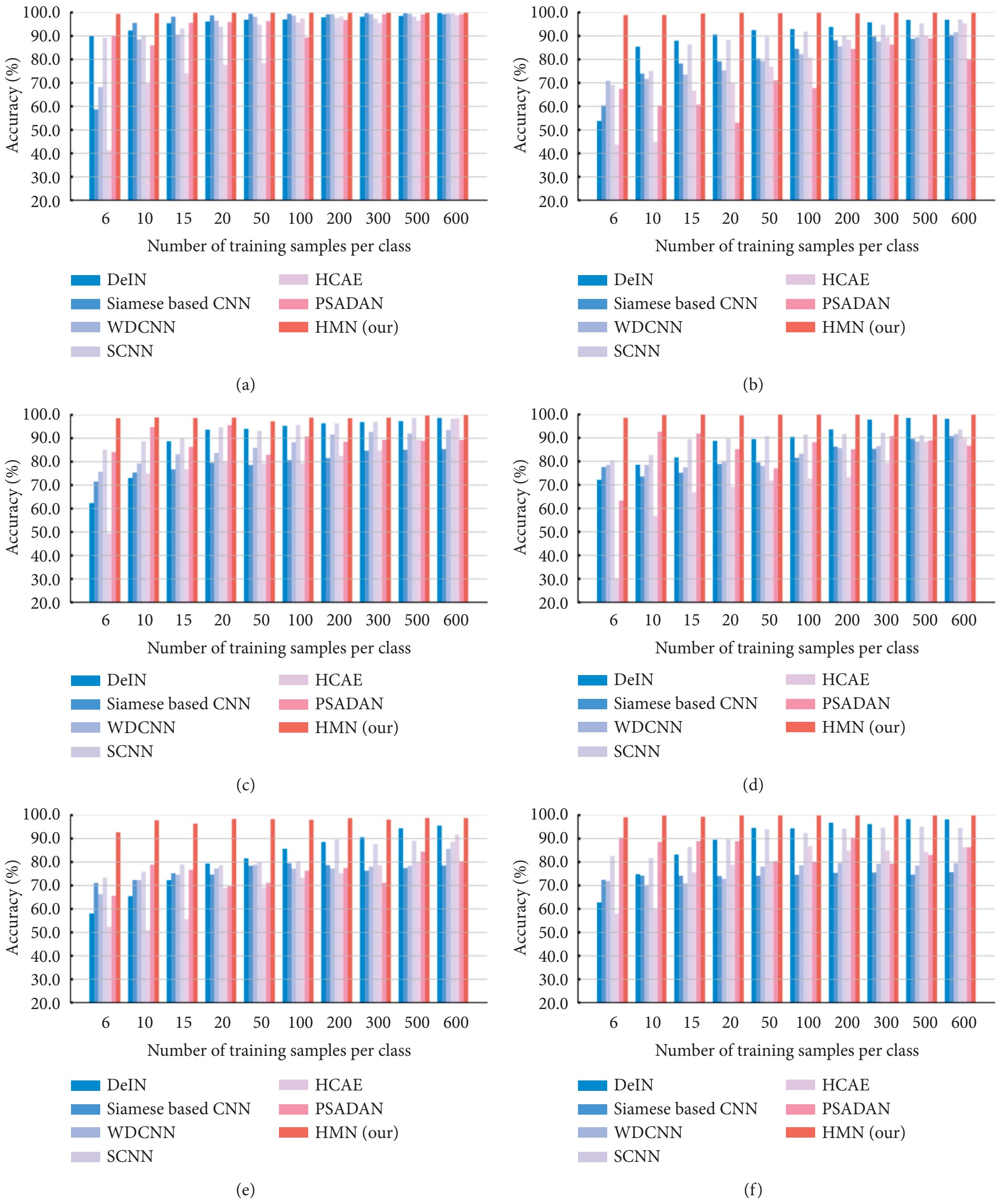

(a)

(b)

(c)

(d)

(e)

(f)

FIGURE 8: The mean classification accuracy with the increasing number of training samples on CWRU. (a) Dataset A to dataset B. (b) Dataset A to dataset C. (c) Dataset B to dataset A. (d) Dataset B to dataset C. (e) Dataset C to dataset A. (f) Dataset C to dataset B.

Based CNN, WDCNN, SCNN, HCAE, and PSDAN, respectively.

In Tables 6 and 7, the precisions and $F1$ ($\alpha F1$) of HMN and the other 6 methods in the cross-domain task C-A are compared, each training class containing 6 samples (the most difficult task). The results reveal that the suggested HMN outperformed all of the compared approaches. This evidenced that HMN can achieve more robust performance in cross-domain diagnostic tasks with limited training samples.

To further evaluate the effectiveness of the proposed method, we observed the effects of the autoencoder and random dropout in improving model's performance through the loss curve. Figures 9 and 10 show the loss curves in cross-domain task C-A with 6 training samples per class.

Table 5: Mean classification accuracy (%) with 6 training samples per class on CWRU.

Methods	A-B	A-C	B-A	B-C	C-A	C-B	Average
DeIN	90.14	53.76	62.33	72.17	58.04	62.76	66.53
Siamese based CNN	58.68	60.40	71.51	77.56	71.08	72.42	68.61
WDCNN	68.17	70.92	75.68	78.44	66.27	71.86	71.89
SCNN	89.14	69.15	85.15	80.44	73.33	82.56	79.96
HCAE	41.33	43.67	49.23	30.16	52.44	57.99	45.80
PSADAN	90.00	67.40	84.07	63.33	65.56	90.37	76.79
HMN (our)	**99.34**	**98.87**	**98.57**	**98.54**	**92.65**	**99.08**	**97.84**

Table 6: Precision (%) comparison for cross-domain task C-A with 6 training samples per training class on CWRU.

	Class 1	Class 2	Class 3	Class 4	Class 5	Class 6	Class 7	Class 8	Class 9	Class 10
DeIN	51.61	63.16	61.90	51.85	65.22	66.67	76.00	60.00	44.44	56.00
Siamese based CNN	75.00	81.48	80.77	67.86	72.73	50.00	65.38	73.91	70.00	80.00
WDCNN	65.38	60.00	64.00	56.52	69.57	77.78	66.67	69.23	66.67	68.42
SCNN	70.00	70.37	69.23	70.83	90.48	74.07	69.23	80.00	71.43	73.91
HCAE	55.56	55.26	40.00	44.00	40.00	52.17	57.69	66.67	54.84	66.67
PSADAN	56.52	84.21	55.56	50.00	61.11	76.92	75.00	72.73	66.67	72.41
HMN (our)	**88.46**	**92.59**	**87.50**	**92.31**	**100.00**	**89.29**	**96.00**	**88.46**	**100.00**	**95.65**

Table 7: $F1$ and $\alpha F1$ (%) comparison with 6 training samples per class for cross-domain task C-A with 6 training samples per class on CWRU.

	Class 1	Class 2	Class 3	Class 4	Class 5	Class 6	Class 7	Class 8	Class 9	Class 10	αF1
DeIN	57.14	54.55	56.52	53.85	62.50	55.81	76.00	60.00	52.46	56.00	58.48
Siamese based CNN	66.67	84.62	82.35	71.70	68.09	52.83	66.67	70.83	76.36	71.11	71.12
WDCNN	66.67	65.45	64.00	54.17	66.67	80.77	65.31	70.59	69.23	59.09	66.19
SCNN	76.36	73.08	70.59	69.39	82.61	76.92	70.59	80.00	65.22	70.83	73.56
HCAE	46.51	66.67	43.64	44.00	35.56	50.00	58.82	55.81	60.71	60.87	52.26
PSADAN	54.17	72.73	57.69	61.54	51.16	78.43	58.54	68.09	72.73	77.78	65.28
HMN (our)	**90.20**	**96.15**	**85.71**	**94.12**	**93.62**	**94.34**	**96.00**	**90.20**	**95.83**	**91.67**	**92.78**

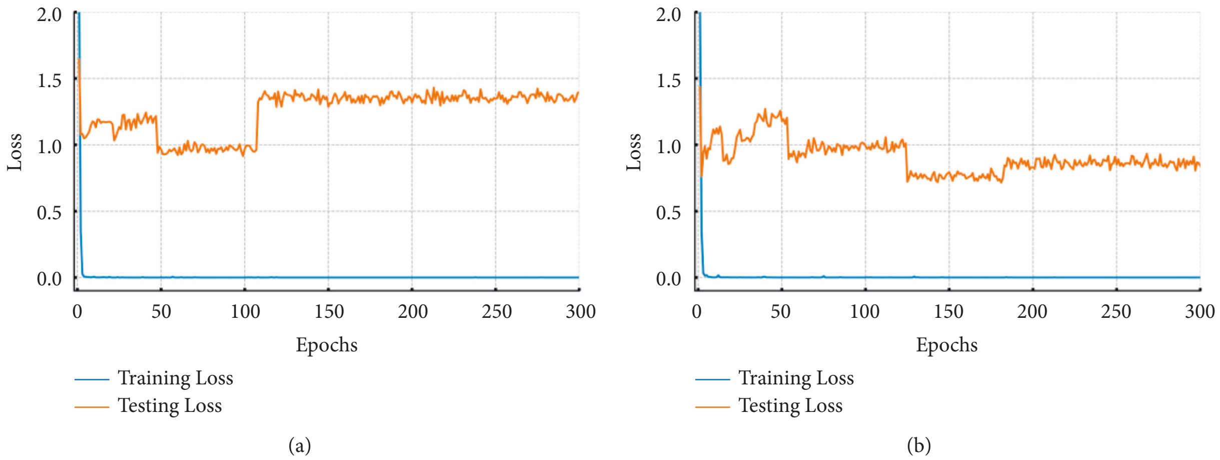

Figure 9: Continued.

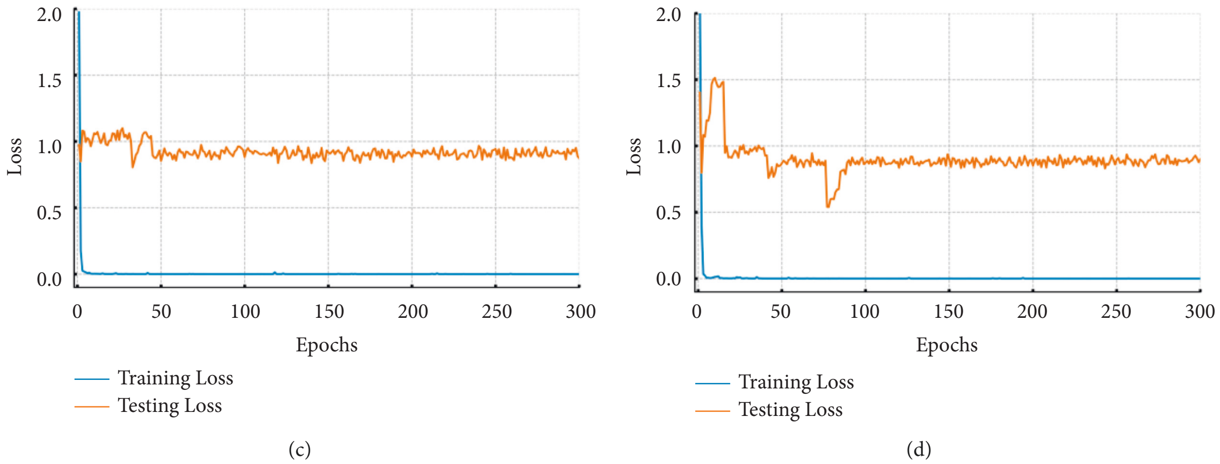

Figure 9: Loss curves of the proposed model when α is set different values in cross-domain task dataset C to dataset A. (a) $\alpha = 0$. (b) $\alpha = 0.2$. (c) $\alpha = 0.5$. (d) $\alpha = 0.8$.

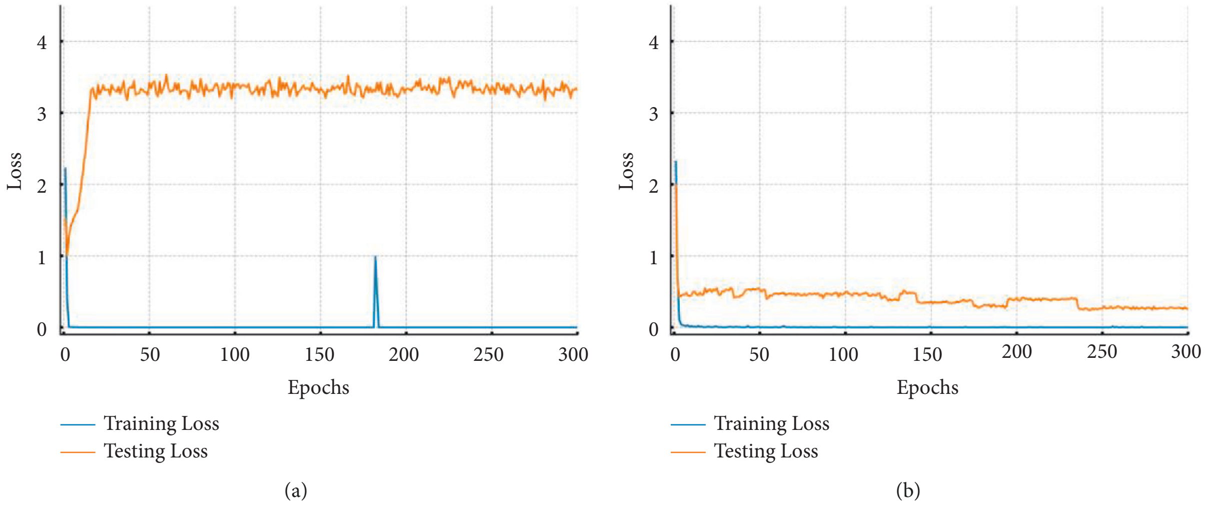

Figure 10: Loss curves: (a) training without random dropout; (b) training with random dropout.

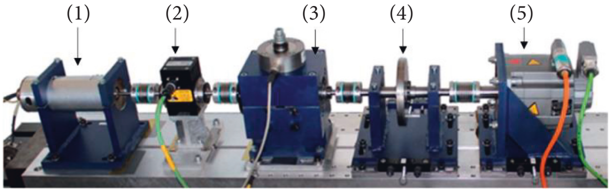

Figure 11: Test rig of Paderborn bearing dataset.

Table 8: Working conditions of rolling bearing on Paderborn.

Datasets	Rotational [rpm]	Load torque [Nm]	Radial force [N]	Name of setting
D	1500	0.7	1000	N15_M07_F10
E	1500	0.1	1000	N15_M01_F10
F	1500	0.7	400	N15_M07 _F04

As shown in Figure 9, training losses containing reconstruction loss L_r and classification loss L_c are considered to originate from equation (9), with testing losses set to classification loss L_c. According to equation (9), when α is set to 0, the autoencoder does not work. A greater α indicates a higher weight of autoencoder during the training process. As α increases from 0 to 0.2, the testing loss converges to a smaller value. The testing loss's convergence process is smoother when α equals to 0.5. This demonstrates how the autoencoder branch may prevent overfitting and improve the model's performance.

As shown in Figure 10, when the HMN does not employ random dropout on input, the convergence value of the testing loss is greater than 3; however, when random dropout is used, the convergence value of testing loss drops to less than 1, and the curve descends more smoothly. The effect of random dropout on input in improving the model's cross-domain generalization is demonstrated.

Table 9: Data sets used for experiments.

Fault location	None	Out race	Inner race
File no.	K001 K002	Artificial (KA01) Real damages (KA04)	Artificial (KI01) Real damages (KI14)

Table 10: Detail of datasets on Paderborn.

Dates sets	Splitting	None (class 1)	Inner race (class 2)	Out race (class 3)
D	Training	600	600	600
	Testing	40	40	40
E	Training	600	600	600
	Testing	40	40	40
F	Training	600	600	600
	Testing	40	40	40

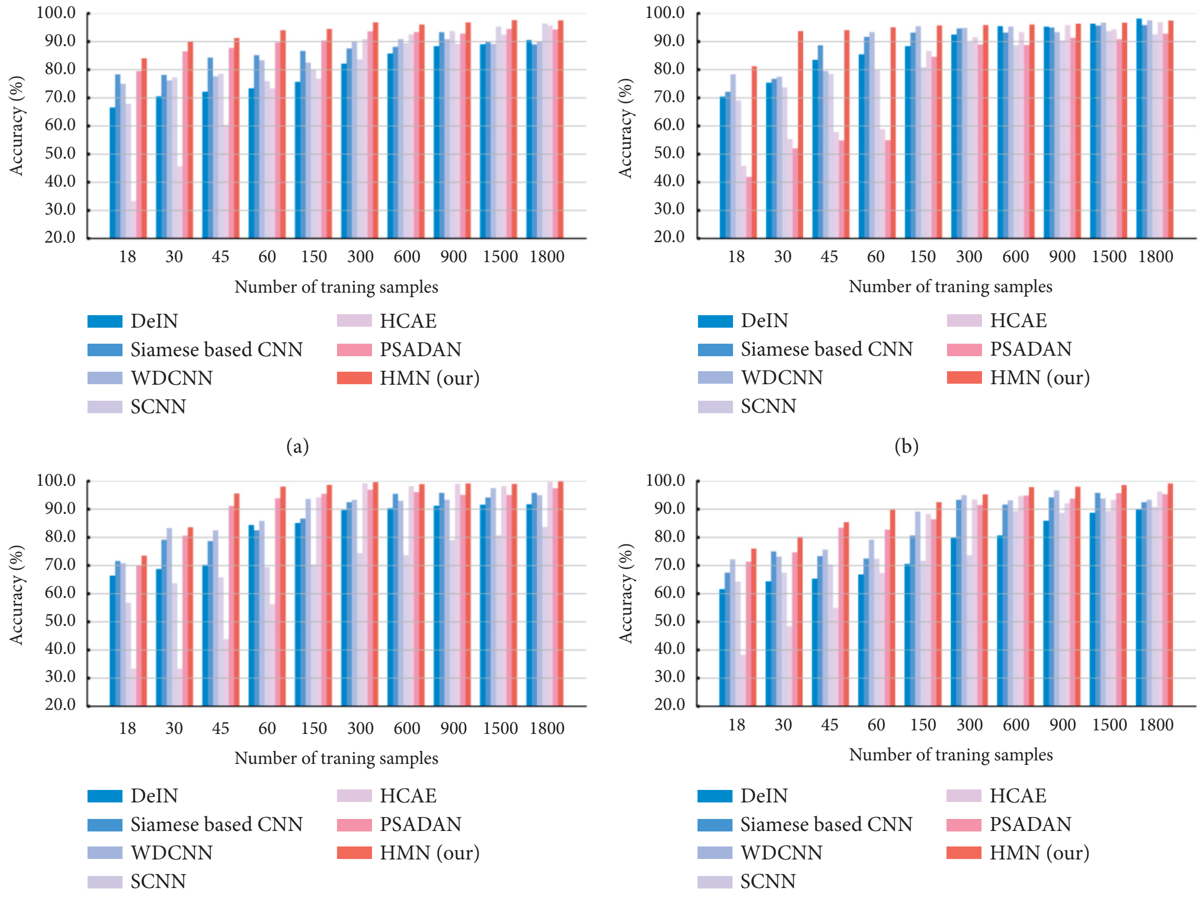

(a)

(b)

(c)

(d)

Figure 12: Continued.

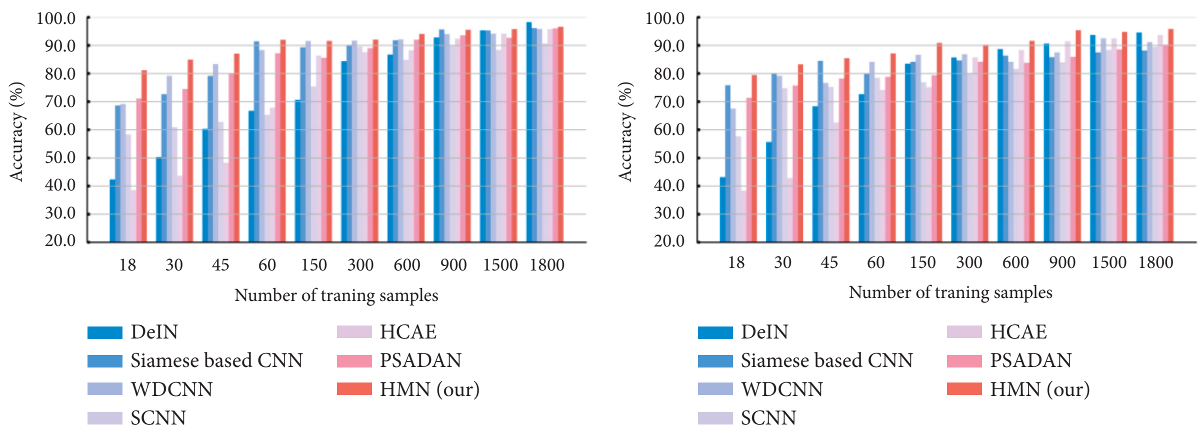

(e)

(f)

Figure 12: The mean classification accuracy with the increasing number of training samples on the Paderborn dataset. (a) Dataset D to dataset E. (b) Dataset D to dataset F. (c) Dataset E to dataset D. (d) Dataset E to dataset F. (e) Dataset F to dataset D. (f) Dataset F to dataset E.

Table 11: Mean classification accuracy (%) comparison with 6 samples per class on the Paderborn dataset.

Methods	D-E	D-F	E-D	E-F	F-D	F-E	Average
DeIN	66.57	70.47	66.41	61.57	42.37	43.21	58.43
Siamese based CNN	78.33	72.16	71.66	67.50	68.66	75.83	72.36
WDCNN	75.00	78.33	70.83	72.16	69.16	67.50	72.16
SCNN	67.83	69.03	56.82	64.27	58.34	57.63	62.32
HCAE	33.34	45.86	33.33	38.33	38.56	38.37	37.97
PSADAN	79.47	41.91	70.16	71.35	71.14	71.36	67.57
HMN (our)	**84.06**	**81.20**	**73.53**	**76.00**	**81.13**	**79.46**	**79.23**

4.3. Case Study 2: Paderborn Dataset

4.3.1. Data Description. As shown in Figure 11, the test rig [44] consists of five modules: (1) electric motor, (2) torque-measurement shaft, (3) rolling bearing test module, (4) flywheel, and (5) load motor. Bearings with different state types were installed in the test module to obtain experimental data. Fault types of bearings come from artificial and real damages.

In the basic setting of operating condition, the test platform ran at $n = 1500$ rpm with a load torque of $M = 0.7$ Nm and a radial force on the bearing of $F = 1{,}000$ N. Other settings were set up by changing the parameters one by one to $M = 0.1$ Nm and $F = 400$ N (named D, E, F, respectively, shown as Table 8.

The bearings with 32 different states were operated under different working conditions, including 14 states with natural damages from accelerated lifetime tests, 12 states with artificial damage, and 6 states with health data.

Each bearing under a load setting is measured with a vibration signal of about 4s at a 64 kHz sampling rate. In the experiment, datasets contained signals obtained from healthy bearings, artificially damaged bearings, and naturally damaged bearings. All bearings of different fault types were running under three different loads at a speed of 1500 rpm. The datasets filenames selected are shown in Table 9. The details of the datasets selected are listed in Table 10. Each dataset contains 1800 training samples and 120 test samples.

Table 12: Precision (%) comparison for cross-domain task E-D with 6 training samples per class on the Paderborn dataset.

	Class 1	Class 2	Class 3
DeIN	62.00	69.23	70.97
Siamese based CNN	81.25	74.36	63.27
WDCNN	67.44	75.76	70.45
SCNN	60.00	56.82	56.10
HCAE	36.36	31.11	33.33
PSADAN	69.04	75.00	68.42
HMN (our)	**75.00**	**76.19**	**71.05**

Table 13: F1 and αF1 (%) comparison for cross-domain task E-D with 6 training samples per class on the Paderborn dataset.

	Class 1	Class 2	Class 3	αF1
DeIN	68.89	68.35	61.97	66.41
Siamese based CNN	72.22	73.42	69.66	71.77
WDCNN	69.88	68.49	**73.81**	70.73
SCNN	56.00	59.52	56.79	57.44
HCAE	32.88	32.94	34.15	33.32
PSADAN	70.73	75.00	66.67	70.80
HMN (our)	**75.00**	**78.05**	69.23	**74.09**

4.3.2. Results and Analysis. By performing the same implementation, Figure 12 compares our method with the compared approaches in terms of the accuracy of different cross-domain tasks. The results show that our method outperformed the other six stat-of-the-art methods in all the scenarios.

Table 11 illustrates the cross-domain tasks accuracy of different methods with 6 training samples per class. The proposed method outperformed all comparative methods by 6.87%–41.26% on average. Tables 12 and 13 compare the methods in terms of precision, $F1$, and $\alpha F1$ in the cross-domain task E-D with 6 training samples per class. The results also show that our method outplay the alternatives.

5. Conclusions

A novel HMN was proposed for cross-domain fault diagnosis with limited training samples. We improved the model's diagnostic performance in two ways: (1) a novel deep learning structure combining autoencoder and matching network was built, (2) a random dropout strategy adding random disturbance into the inputs during the training process was developed to enhance the model's domain generalization. In Section 4, we present the experimental results showing that the proposed method has better domain generalization ability with limited training samples compared with the state-of-the-art approaches.

However, the method proposed in this study still has some restrictions. For example, the method is limited to cross-domain tasks between different working conditions on the same device. However, cross-domain across multiple devices makes intelligent fault diagnosis algorithms more realistic. In addition, HMN can only perform classification tasks, limiting the model's potential to multitask. In future work, we will further optimize HMN and employ it in more complex cross-domain fault diagnosis scenarios and multitask learning.

Data Availability

The data used to support the findings of this study are available from the corresponding author upon request.

Conflicts of Interest

The authors declare no conflicts of interest.

Acknowledgments

This work was supported in part by the National Key Research and Development Program (grant number 2020YFB1713300), the National Key Technologies Research and Development Program of China (grant number 2018AAA0101803), the National Natural Science Foundation of China (grant number 91746116), the Science and Technology Project of Guizhou Province Talents (grant numbers (2015)4011 and (2017)5788), the Guizhou Province University Talent Training Base Project (grant number (2020)009), the Guizhou Science and Technology Planning Project (grant number (2017)3001), the Guizhou Optoelectronic Information and Intelligent Application International Joint Research Center (grant number (2019) 5802), and the Guizhou Province University Integration Research Platform Project (grant number (2020)005).

References

[1] A. Dibaj, M. M. Ettefagh, R. Hassannejad, and M. B. Ehghaghi, “A hybrid fine-tuned VMD and CNN scheme for untrained compound fault diagnosis of rotating machinery with unequal-severity faults,” *Expert Systems with Applications*, vol. 167, Article ID 114094, 2021.

[2] B. Cai, K. Hao, Z. Wang et al., “Data-driven early fault diagnostic methodology of permanent magnet synchronous motor,” *Expert Systems with Applications*, vol. 177, Article ID 115000, 2021.

[3] X. Yaoyu, L. Yuan, W. Yijing, Z. Dexing, and Z. Guanjun, “Improved few-shot learning method for transformer fault diagnosis based on approximation space and belief functions [J],” *Expert Systems with Applications*, vol. 167, Article ID 114105, 2021.

[4] Q. Bai, S. Li, J. Yang, Q. Song, Z. Li, and X. Zhang, “Object detection recognition and robot grasping based on machine learning: a survey,” *IEEE Access*, vol. 8, pp. 181855–181879, 2020.

[5] M. A. Morid, A. Borjali, and G. Del Fiol, “A scoping review of transfer learning research on medical image analysis using ImageNet,” *Computers in Biology and Medicine*, vol. 128, Article ID 104115, 2021.

[6] E. M. Davidson, M. T. C. Poon, A. Casey et al., “The reporting quality of natural language processing studies: systematic review of studies of radiology reports,” *BMC Medical Imaging*, vol. 21, no. 1, p. 142, 2021.

[7] J. Yang, S. Li, Z. Wang, and G. Yang, “Real-time tiny part defect detection system in manufacturing using deep learning,” *IEEE Access*, vol. 7, pp. 89278–89291, 2019.

[8] X. Ran, X. Zhou, M. Lei, W. Tepsan, and W. Deng, “A novel k-means clustering algorithm with a noise algorithm for capturing urban hotspots,” *Applied Sciences*, vol. 11, no. 23, Article ID 11202, 2021.

[9] K. Zhang, B. Tang, L. Deng, Q. Tan, and H. Yu, “A fault diagnosis method for wind turbines gearbox based on adaptive loss weighted meta-ResNet under noisy labels,” *Mechanical Systems and Signal Processing*, vol. 161, Article ID 107963, 2021.

[10] Q. Ni, J. Ji, K. Feng, and B. Halkon, “A novel correntropy-based band selection method for the fault diagnosis of bearings under fault-irrelevant impulsive and cyclostationary interferences,” *Mechanical Systems and Signal Processing*, vol. 153, Article ID 107498, 2021.

[11] H. Wang, C. Liu, D. Jiang, and Z. Jiang, “Collaborative deep learning framework for fault diagnosis in distributed complex systems,” *Mechanical Systems and Signal Processing*, vol. 156, Article ID 107650, 2021.

[12] Y. Sun, S. Li, Y. Wang, and X. Wang, “Fault diagnosis of rolling bearing based on empirical mode decomposition and improved manhattan distance in symmetrized dot pattern image,” *Mechanical Systems and Signal Processing*, vol. 159, Article ID 107817, 2021.

[13] S. Pang, X. Yang, X. Zhang, and Y. Sun, “Fault diagnosis of rotating machinery components with deep ELM ensemble induced by real-valued output-based diversity metric,” *Mechanical Systems and Signal Processing*, vol. 159, Article ID 107821, 2021.

[14] Z. Feng, A. Gao, K. Li, and H. Ma, "Planetary gearbox fault diagnosis via rotary encoder signal analysis," *Mechanical Systems and Signal Processing*, vol. 149, Article ID 107325, 2021.

[15] X. Wen and Z. Xu, "Wind turbine fault diagnosis based on ReliefF-PCA and DNN," *Expert Systems with Applications*, vol. 178, Article ID 115016, 2021.

[16] M. J. Hasan, A. Rai, Z. Ahmad, and J.-M. Kim, "A fault diagnosis framework for centrifugal pumps by scalogram-based imaging and deep learning," *IEEE Access*, vol. 9, pp. 58052–58066, 2021.

[17] M. J. Hasan, M. Sohaib, and J.-M. Kim, "An explainable ai-based fault diagnosis model for bearings," *Sensors*, vol. 21, no. 12, p. 4070, 2021.

[18] W. Sun, S. Shao, R. Zhao, R. Yan, X. Zhang, and X. Chen, "A sparse auto-encoder-based deep neural network approach for induction motor faults classification," *Measurement*, vol. 89, pp. 171–178, 2016.

[19] C. Li, R.-V. Sanchez, G. Zurita, M. Cerrada, D. Cabrera, and R. E. Vásquez, "Gearbox fault diagnosis based on deep random forest fusion of acoustic and vibratory signals," *Mechanical Systems and Signal Processing*, vol. 76-77, pp. 283–293, 2016.

[20] X. Ding and Q. He, "Energy-fluctuated multiscale feature learning with deep convnet for intelligent spindle bearing fault diagnosis," *IEEE Transactions on Instrumentation and Measurement*, vol. 66, no. 8, pp. 1926–1935, 2017.

[21] W. Zhang, C. Li, G. Peng, Y. Chen, and Z. Zhang, "A deep convolutional neural network with new training methods for bearing fault diagnosis under noisy environment and different working load," *Mechanical Systems and Signal Processing*, vol. 100, pp. 439–453, 2018.

[22] M. Qiao, S. Yan, X. Tang, and C. Xu, "Deep convolutional and LSTM recurrent neural networks for rolling bearing fault diagnosis under strong noises and variable loads," *IEEE Access*, vol. 8, pp. 66257–66269, 2020.

[23] R. Liu, B. Yang, E. Zio, and X. Chen, "Artificial intelligence for fault diagnosis of rotating machinery: a review," *Mechanical Systems and Signal Processing*, vol. 108, pp. 33–47, 2018.

[24] R. Zhao, R. Yan, Z. Chen, K. Mao, P. Wang, and R. X. Gao, "Deep learning and its applications to machine health monitoring," *Mechanical Systems and Signal Processing*, vol. 115, pp. 213–237, 2019.

[25] H. Zhiyi, S. Haidong, J. Lin, C. Junsheng, and Y. Yu, "Transfer fault diagnosis of bearing installed in different machines using enhanced deep auto-encoder," *Measurement*, vol. 152, Article ID 107393, 2020.

[26] B. Yang, Y. Lei, F. Jia, and S. Xing, "An intelligent fault diagnosis approach based on transfer learning from laboratory bearings to locomotive bearings," *Mechanical Systems and Signal Processing*, vol. 122, pp. 692–706, 2019.

[27] H. Cui, Y. Guan, H. Chen, and W. Deng, "A novel advancing signal processing method based on coupled multi-stable stochastic resonance for fault detection," *Applied Sciences*, vol. 11, no. 12, p. 5385, 2021.

[28] M. J. Hasan, M. M. M. Islam, and J.-M. Kim, "bearing fault diagnosis using multidomain fusion-based vibration imaging and multitask learning," *Sensors*, vol. 22, no. 1, p. 56, 2021.

[29] D. Yao, H. Liu, J. Yang, and X. Li, "A lightweight neural network with strong robustness for bearing fault diagnosis," *Measurement*, vol. 159, Article ID 107756, 2020.

[30] T. Hu, T. Tang, R. Lin, M. Chen, S. Han, and J. Wu, "A simple data augmentation algorithm and a self-adaptive convolutional architecture for few-shot fault diagnosis under different working conditions," *Measurement*, vol. 156, Article ID 107539, 2020.

[31] N. Lu and T. Yin, "Transferable common feature space mining for fault diagnosis with imbalanced data," *Mechanical Systems and Signal Processing*, vol. 156, Article ID 107645, 2021.

[32] J. Wu, Z. Zhao, C. Sun, R. Yan, and X. Chen, "Few-shot transfer learning for intelligent fault diagnosis of machine," *Measurement*, vol. 166, Article ID 108202, 2020.

[33] D. Wei, T. Han, F. Chu, and M. J. Zuo, "Weighted domain adaptation networks for machinery fault diagnosis," *Mechanical Systems and Signal Processing*, vol. 158, Article ID 107744, 2021.

[34] J. Wang, Y. Liang, Y. Zheng, R. X. Gao, and F. Zhang, "An integrated fault diagnosis and prognosis approach for predictive maintenance of wind turbine bearing with limited samples," *Renewable Energy*, vol. 145, pp. 642–650, 2020.

[35] A. Zhang, S. Li, Y. Cui, W. Yang, R. Dong, and J. Hu, "Limited data rolling bearing fault diagnosis with few-shot learning," *IEEE Access*, vol. 7, pp. 110895–110904, 2019.

[36] C. Li, S. Li, A. Zhang, Q. He, Z. Liao, and J. Hu, "Meta-learning for few-shot bearing fault diagnosis under complex working conditions," *Neurocomputing*, vol. 439, no. 2, pp. 197–211, 2021.

[37] Q. Hang, J. Yang, and L. Xing, "Diagnosis of rolling bearing based on classification for high dimensional unbalanced data," *IEEE Access*, vol. 7, pp. 79159–79172, 2019.

[38] Q. Li, B. Tang, L. Deng, Y. Wu, and Y. Wang, "Deep balanced domain adaptation neural networks for fault diagnosis of planetary gearboxes with limited labeled data," *Measurement*, vol. 156, Article ID 107570, 2020.

[39] L. Duan, M. Xie, T. Bai, and J. Wang, "A new support vector data description method for machinery fault diagnosis with unbalanced datasets," *Expert Systems with Applications*, vol. 64, pp. 239–246, 2016.

[40] J. Snell, K. Swersky, and R. S. Zemel, "Prototypical networks for few-shot learning," 2017, https://arxiv.org/abs/1703.05175.

[41] N. Srivastava, G. Hinton, A. Krizhevsky, I. Sutskever, and R. Salakhutdinov, "Dropout: a simple way to prevent neural networks from overfitting," *Journal of Machine Learning Research*, vol. 15, no. 1, pp. 1929–1958, 2014.

[42] X. Wu, Y. Zhang, C. Cheng, and Z. Peng, "A hybrid classification autoencoder for semi-supervised fault diagnosis in rotating machinery," *Mechanical Systems and Signal Processing*, vol. 149, Article ID 107327, 2021.

[43] W. A. Smith and R. B. Randall, "Rolling element bearing diagnostics using the Case Western Reserve University data: a benchmark study," *Mechanical Systems and Signal Processing*, vol. 64-65, pp. 100–131, 2015.

[44] C. Lessmeier, J. K. Kimotho, D. Zimmer, and W. Sextro, "Condition monitoring of bearing damage in electromechanical drive systems by using motor current signals of electric motors: a benchmark data set for data-driven classification," in *Proceedings of the European conference of the prognostics and health management society*, pp. 05–08, Citeseer, Turin, Italy, July 2016.

[45] Y. Qin, Q. Yao, Y. Wang, and Y. Mao, "Parameter sharing adversarial domain adaptation networks for fault transfer diagnosis of planetary gearboxes," *Mechanical Systems and Signal Processing*, vol. 160, Article ID 107936, 2021.

[46] W. Zhang, G. Peng, C. Li, Y. Chen, and Z. Zhang, "A new deep learning model for fault diagnosis with good anti-noise and domain adaptation ability on raw vibration signals," *Sensors*, vol. 17, no. 2, p. 425, 2017.

[47] S. Li, W. Yang, A. Zhang et al., "A novel method of bearing fault diagnosis in time-frequency graphs using Inception-Resnet and deformable convolution networks," *IEEE Access*, vol. 8, pp. 92743–92753, 2020.